Applied Nanoscience (2020) 10:3035–3043
https://doi.org/10.1007/s13204-019-01037-x

ORIGINAL ARTICLE

Theoretical and analytical analysis of shear rheology of Oldroyd-B fluid with homogeneous–heterogeneous reactions

Sadia Rashid[1] · M. Ijaz Khan[1] · T. Hayat[1,2] · M. Ayub[1] · A. Alsaedi[2]

Received: 17 January 2019 / Accepted: 9 April 2019 / Published online: 24 April 2019

Abstract

This research article communicates an analytical investigation for the three-dimensional steady incompressible flow of Oldroyd-B fluid subject to stretchable surface. The flow of material induced through stretchable surface with Darcy-Forchheimer medium. Homogeneous–heterogeneous reactions is considered. Convective boundary conditions and heat source/sink effects are considered for the heat transport. Boundary layer concept is used in the development of flow problem. Series solutions are obtained of the nonlinear system through homotopy technique. Physical significance of pertinent parameters are discussed and plotted graphically. Heat transfer rate is discussed numerically.

Keywords Oldroyd-B fluid · Darcy-Forchheimer porous medium · Heat source/sink · Homogeneous–heterogeneous reactions · Convective boundary conditions

Introduction

Non Newtonian materials play an imperative role in frequent mechanical and industrial engineering and branches of applied science. The non-Newtonian materials are divided into three different categories, namely integral, differential and rate types. There are numerous non-Newtonian material models like Jeffrey model, Eyring model, Prandtl Eyring model, Casson model, second grade, Sisko model, Oldroyd-B model, Carreaue model and so on. Here we have considered Oldroyd-B model which is a rate material that exhibits properties of retardation and relaxation times. Zhang et al. (2016) discussed heat transport characteristics in flow of Oldroyd-B nanoliquid subject to time-dependent thin-film stretchable sheet. Shivakumara et al. (2015) scrutinized thermal convective instability in nanoliquid flow of Oldroyd-B fluid over a porous medium. Forced convective nanomaterial flow of Oldroyd-B fluid between two isothermal stretchable disks with magnetic field is examined by Hashmi et al. (2017). Zhang et al. (2018) explored thin-flim flow of Oldroyd-B nanoliquid with Cattaneo-Christov double diffusion. They also considered chemical reaction and dissipation effects. Shehzad et al. (2014) scrutinized 3D-forced convective Oldroyd-B fluid flow with thermophoresis and Brownian diffusions. Kumar et al. (2018) worked on the nanomaterial flow of Oldroyd-B fluid subject to radiative flux and dissipation. Electrical conducting nanomaterial flow of non-Newtonian liquid subject to porous stretchable sheet is investigated by Das et al. (2018). Gireesha et al. (2018) discussed heat and mass transport in nanoliquid flow of Oldroyd-B material with heat source/sink by a stretchable surface. Khan and Mahmood (2016) discussed combined effects of heat source/sink and thermophoretic diffusion in nanoliquid flow of non-Newtonian fluid inside stretchable disks. Flow of Oldroyd-B nanomaterial with heat source/sink and radiative flux is explored by Waqas et al. (2017a). Refs. Shehzad (2018), Hayat et al. (2016a, b, 2017a, b, c, d, e, 2018a, b), Khan et al. (2016, 2017a, b, c, d, e, f, 2018a, b), Muhammad et al. (2017), Ellahi et al. (2014a, b, 2016), Meraj et al. (2017), Alamri et al. (2019), Akbarzadeh et al. (2018), Hassan et al. 2018), Rashidi et al. (2018), Tamoor et al. (2017), Waqas et al. (2017b) represent various fluid models subject to different flow assumptions.

Keeping such effectiveness in mind, we have considered 3D cubic chemical reactive flow of Oldroyd-B material

✉ M. Ijaz Khan
ijazqau_khan@yahoo.com

[1] Department of Mathematics, Quaid-I-Azam University, 45320, Islamabad 44000, Pakistan

[2] Nonlinear Analysis and Applied Mathematics (NAAM) Research Group, Department of Mathematics, Faculty of Science, King Abdul-Aziz University, P. O. Box 80203, Jeddah 21589, Saudi Arabia

subject to Darcy-Forchheimer porous medium. Series solutions are developed through homotopy technique (Shirkhani et al. 2018; Hayat et al. 2017f; Fagbade et al. 2018; Khan et al. 2017g, h, 2018c; Skoneczny and Skoneczny 2018; Khan et al. 2019; Naghshband and Araghi 2018; Hayat et al. 2018c, d, e; Raftari and Vajravelu 2012; Xinhui et al. 2012; Han et al. 2014; Turkyilmazoglu 2010a, b, 2014; Ahmad et al. 2018; Abbasi et al. 2019). Heat transfer rate is deliberated in tabular form.

Modeling

The cubic autocatalysis at the surface is defined as follows:

$$A^* + 2B^* \rightarrow 3B^*, \;\; \text{rate} = k_c a^{**} b^2, \tag{1}$$

and

$$A^* \rightarrow B^*, \;\; \text{rate} = k_s a^{**}, \tag{2}$$

where a^{**} and b, respectively, indicate the concentrations of species A^* and B^* and k_c and k_s are the rate constants.

In component form, the flow equations are as defined by Shehzad et al. (2014):

$$\frac{\partial u}{\partial x} + \frac{\partial v}{\partial y} + \frac{\partial w}{\partial z} = 0, \tag{3}$$

$$\left.\begin{aligned} & u\frac{\partial u}{\partial x} + v\frac{\partial u}{\partial y} + w\frac{\partial u}{\partial z} + \lambda_1\left(\begin{array}{c} u^2\frac{\partial^2 u}{\partial x^2} + v^2\frac{\partial^2 u}{\partial y^2} + w^2\frac{\partial^2 u}{\partial z^2} + 2uv\frac{\partial^2 u}{\partial x\partial y} \\ +2vw\frac{\partial^2 u}{\partial y\partial z} + 2uw\frac{\partial^2 u}{\partial x\partial z} \end{array}\right) \\ & -\nu\left[\frac{\partial^2 u}{\partial z^2} + \lambda_2\left(\begin{array}{c} u\frac{\partial^3 u}{\partial x\partial z^2} + v\frac{\partial^3 u}{\partial y\partial z^2} + w\frac{\partial^3 u}{\partial z^3} \\ -\frac{\partial u}{\partial x}\frac{\partial^2 u}{\partial z^2} - \frac{\partial u}{\partial y}\frac{\partial^2 v}{\partial z^2} - \frac{\partial u}{\partial z}\frac{\partial^2 w}{\partial z^2} \end{array}\right)\right] - \frac{\nu}{K}u - Fu^2 = 0 \end{aligned}\right\}, \tag{4}$$

$$\left.\begin{aligned} & u\frac{\partial v}{\partial x} + v\frac{\partial v}{\partial y} + w\frac{\partial v}{\partial z} + \lambda_1\left(\begin{array}{c} u^2\frac{\partial^2 v}{\partial x^2} + v^2\frac{\partial^2 v}{\partial y^2} + w^2\frac{\partial^2 v}{\partial z^2} \\ +2uv\frac{\partial^2 v}{\partial x\partial y} + 2vw\frac{\partial^2 v}{\partial y\partial z} + 2uw\frac{\partial^2 v}{\partial x\partial z} \end{array}\right) \\ & -\nu\left[\frac{\partial^2 v}{\partial z^2} + \lambda_2\left(\begin{array}{c} u\frac{\partial^3 v}{\partial x\partial z^2} + v\frac{\partial^3 v}{\partial y\partial z^2} + w\frac{\partial^3 v}{\partial z^3} \\ -\frac{\partial v}{\partial x}\frac{\partial^2 u}{\partial z^2} - \frac{\partial v}{\partial y}\frac{\partial^2 v}{\partial z^2} - \frac{\partial v}{\partial z}\frac{\partial^2 w}{\partial z^2} \end{array}\right)\right] - \frac{\nu}{K}v - Fv^2 \end{aligned}\right\}, \tag{5}$$

$$u\frac{\partial T}{\partial x} + v\frac{\partial T}{\partial y} + w\frac{\partial T}{\partial z} = \frac{k}{\rho c_p}\frac{\partial^2 T}{\partial z^2} + \frac{Q_0}{\rho c_p}\left(T - T_\infty\right), \tag{6}$$

$$u\frac{\partial a^{**}}{\partial x} + v\frac{\partial a^{**}}{\partial y} + w\frac{\partial a^{**}}{\partial z} = D_A\frac{\partial^2 a^{**}}{\partial z^2} - k_c a^{**} b^2, \tag{7}$$

$$u\frac{\partial b}{\partial x} + v\frac{\partial b}{\partial y} + w\frac{\partial b}{\partial z} = D_B\frac{\partial^2 a}{\partial z^2} + k_c a^{**} b^2, \tag{8}$$

With

$$\left.\begin{array}{c} u = u_w(x) = ax, \; v = 0, \; w = 0, \; -k\frac{\partial T}{\partial z} = h_f\left(T_f - T\right) \;\text{at}\, z = 0 \\ D_A\frac{\partial a^{**}}{\partial z} = k_s a^{**}, \; D_B\frac{\partial b}{\partial z} = -k_s a^{**} \;\text{at}\; z = 0 \\ u \rightarrow 0, \; v \rightarrow 0, \;\; T \rightarrow T_\infty, \; a^{**} \rightarrow a_0, \; b \rightarrow 0 \;\text{at}\; z = \infty \end{array}\right\}, \tag{9}$$

where x, y, z denote the Cartesian coordinates, u, v, w velocity components, ρ the density, ν the kinematic viscosity, λ_1 and λ_2 represent the relaxation and retardation time, $F\left(= \frac{C_b}{K^{1/2}}\right)$ the coefficient of non-uniform inertia, $\nu = \left(\frac{\mu}{\rho}\right)$ the kinematic viscosity, K the permeability of porous medium, C_b the drag coefficient, T is constant surface temperature, k the thermal conductivity, c_p the specific heat, T_∞ the ambient temperature, Q_0 the heat source/sink coefficient, D_A and D_B the diffusion coefficients, a_0 the positive constant and T_f, h_f the fluid temperature and heat transfer coefficient.

Considering

$$\left.\begin{array}{l} \zeta = \sqrt{\frac{a}{\nu}}z, \; u = axf'(\zeta), \;\; v = ayg(\zeta), \;\; w = -(a\nu)^{\frac{1}{2}}f(\zeta), \\ \theta(\zeta) = \frac{T - T_\infty}{T_f - T_\infty}, \;\; a^{**} = a_0\phi(\zeta), \;\; b = a_0 h(\zeta) \end{array}\right\}. \tag{10}$$

we have

$$\begin{aligned} & f''' + \Lambda f' + \beta_1\left(2ff'f'' - f^2 f'''\right) \\ & \quad + ff'' + \beta_2\left(f''^2 - f'f^{(4)}\right) - \left(1 + F_r\right)f'^2 = 0, \end{aligned} \tag{11}$$

$$\begin{aligned} & g'' - \Lambda g + fg' - f'g + \beta_1\left(2ff'g' - f^2 g''\right) \\ & \quad + \beta_2\left(f'g'' - fg''' - gf''' + g'f''\right) - F_r g^2 = 0, \end{aligned} \tag{12}$$

$$\theta'' + \Pr\left(f\theta' + S\theta\right) = 0, \tag{13}$$

$$\frac{1}{Sc}\phi'' + f\phi' - k_1 h^2\phi = 0, \tag{14}$$

$$\frac{1}{Sc}h'' + fh' + k_1 h^2\phi = 0, \tag{15}$$

$$\left.\begin{array}{l} f = 0 = g, f' = 1, \theta'(0) = -\gamma(1 - \theta(0)), \phi'(0) = k_2\phi(0), \\ \delta h'(0) = -k_2\phi(0), \\ f'(\infty) \rightarrow 0, g(\infty) \rightarrow 0, \theta(\infty) \rightarrow 0, \; \phi(\infty) \rightarrow 1, h(\infty) \rightarrow 0 \end{array}\right\}, \tag{16}$$

where $\Lambda\left(= \frac{\nu}{Ka}\right)$ denotes porosity parameter, $Fr\left(= \frac{C_b}{K^{\frac{1}{2}}}\right)$ the inertial coefficient variable, $\beta_1\left(= \lambda_1 a\right)$ the fluid relaxation, $\beta_2\left(= \lambda_2 a\right)$ the fluid retardation, $Pr\left(= \frac{\nu}{\alpha}\right)$ the Prandtl number, $\gamma\left(=\frac{h_f}{k}\sqrt{\frac{\nu}{a}}\right)$ the Biot number, $S\left(=\frac{Q_0}{a\rho c_p}\right)$ the heat source/sink parameter, $Sc\left(=\frac{\nu}{D_A}\right)$ the Schmidt number, $k_1\left(=\frac{k_c a_0^2}{a}\right)$ the homogeneous strength variable, $k_2\left(=\frac{k_s}{D_A}\sqrt{\frac{\nu}{a}}\right)$ the heterogeneous strength variable, $\delta\left(=\frac{D_B}{D_A}\right)$ the diffusion parameter.

For comparable mass diffusions we put D_A and D_B as equal; we have

$$\phi(\zeta) + h(\zeta) = 1; \tag{17}$$

one has

$$\frac{1}{Sc}\phi'' + f\phi' - k_1(1-\phi)^2\phi = 0, \tag{18}$$

with

$$\phi'(0) = k_2\phi(0),\ \ \phi(\infty) \to 1. \tag{19}$$

The heat transfer rate is mathematically defined as

$$Nu_x = \frac{xq_w}{k\left(Tw - T_\infty\right)}, \tag{20}$$

where hall flux is defined as

$$q_w = -k\frac{\partial T}{\partial z}\ |_{z=o}, \tag{21}$$

Finally, one has

$$Nu_x Re_x^{-0.5} = -\theta'(0), \tag{22}$$

where $Re_x\left(=\frac{u_w x}{\nu}\right)$ symbolizes the local Reynolds number.

Solution procedure

We have

$$\left.\begin{aligned} f_0(\zeta) &= 1 - e^{-\zeta},\\ g_0(\zeta) &= 0,\\ \theta_0(\zeta) &= \frac{\gamma}{1+\gamma}e^{-\zeta},\\ \phi_0(\zeta) &= 1 - \frac{1}{2}e^{-k_2\zeta}, \end{aligned}\right\}, \tag{23}$$

$$\left.\begin{aligned} L_f(\zeta) &= f''' - f',\ L_g = g'' - g,\\ L_\theta(\zeta) &= \theta'' - \theta,\ L_\phi = \phi'' - \phi, \end{aligned}\right\}, \tag{24}$$

with the following characteristics:

$$\left.\begin{aligned} L_f\left[A_{*1} + A_{*2}e^{-\zeta} + A_{*3}e^{\zeta}\right] &= 0,\\ L_g\left[A_{*5}e^{-\zeta} + A_{*5}e^{\zeta}\right] &= 0,\\ L_\theta\left[A_{*6}e^{-\zeta} + A_{*7}e^{\zeta}\right] &= 0,\\ L_\phi\left[A_{*8}e^{-\zeta} + A_{*9}e^{\zeta}\right] &= 0, \end{aligned}\right\}, \tag{25}$$

where $A_{*i}(i = 1-9)$ designates are arbitrary constants

$$\left.\begin{aligned} A_{*2} &= A_{*4} = A_{*6} = A_{*8} = 0,\\ A_{*1} &= -A_{*3} - f_m^*(0),\ A_{*3} = \frac{\partial f_m^*(\zeta)}{\partial\zeta}\ |_{\zeta=0},\ A_{*5} = -\frac{\partial g_m^*(\zeta)}{\partial\zeta}\ |_{\zeta=0},\\ A_{*7} &= \frac{1}{1+\gamma}\left[\frac{\partial\theta_m^*(\zeta)}{\partial\zeta}\ |_{\zeta=0} - \gamma\left(\theta_m^*(0)\right)\right],\\ A_{*9} &= \frac{1}{1+k_2}\left[\frac{\partial\phi_m^*(\zeta)}{\partial\zeta}\ |_{\zeta=0} - k_2\left(\phi_m^*(0)\right)\right] \end{aligned}\right\}. \tag{26}$$

Convergence analysis

In series solutions auxiliary variables $h_f, h_g, h_\theta, h_\phi$ play an important role to adjust the convergence portion. Therefore, we have plotted h - curves for such analysis in Figs. 1 and 2. From these plots the valuable ranges are $-1.8 \le h_f \le -0.1$, $-1.6 \le h_g \le -0.1$, $-2.1 \le h_\theta \le 0.1$ and $-2.1 \le h_\varphi \le 0.1$. Table 1 is sketched for the numerical iterations of convergence analysis.

Discussion

This section is established to explore the impacts of interesting variables on velocity, temperature and concentration fields. For this purpose we have plotted Figs. 3, 4, 5, 6, 7, 8, 9, 10, 11, 12, 13, 14, 15, 16, 17, 18. Porosity variable behavior on velocity $f'(\xi)$ is presented in Fig. 3. Velocity diminishes versus larger porosity variable. Physically, due to porous media, more resistance occurred to the flow particles which make the velocity of fluid weaker. In Fig. 4, we have plotted the impact of fluid relaxation variable on velocity field. Here we observed that the velocity of material particles enhances versus larger relaxation variable. Furthermore, boundary layer shows an increasing impact against larger relaxation variable. Figure 5 is outlined to show the velocity field against retardation variable. Here we noticed that velocity field declines via higher retardation parameter. Inertia variable impact on velocity field is highlighted in Fig. 6. Here velocity curves slowly increase when the inertia variable takes the maximum range. Also layer thickness upsurges versus larger inertia variable. Inspiration of porosity variable on $g(\xi)$ is depicted in Fig. 7. Here initially velocity of liquid particles increases and then shows decreasing impact when the porosity variable take the maximum values. Salient aspects of relaxation and retardation variable on $g(\xi)$ is outlined in Figs. 8 and 9. From these sketches we can see that velocity field monotonically decays initially near the stretchable surface and then monotonically upsurges against larger relaxation and retardation variables. Figure 10 is revealed for the impact of Forchheimer number or inertia coefficient

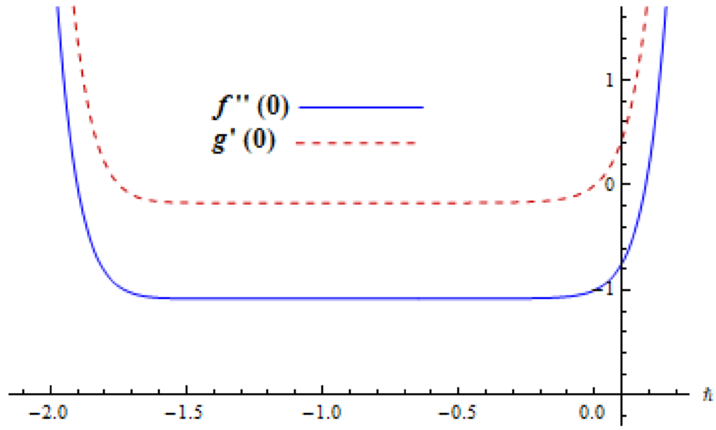

Fig. 1 h - curves for $f''(0)$and$g'(0)$

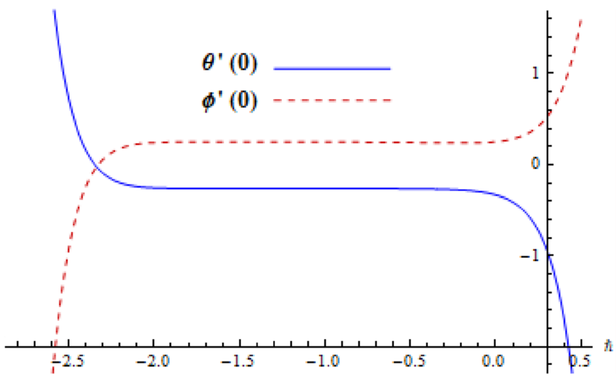

Fig. 2 h - curves for$\theta'(0)$and$\phi'(0)$

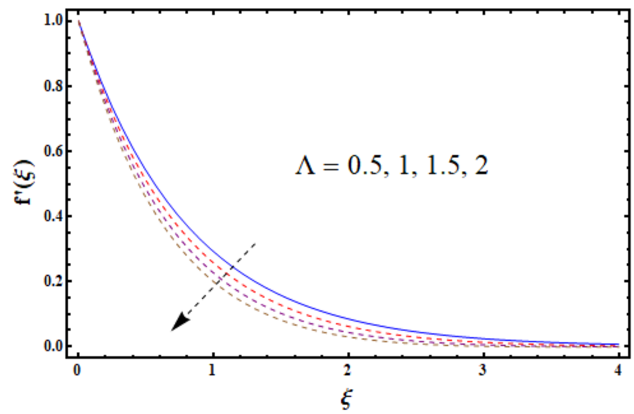

Fig. 3 f'versus Λ

Table 1 Different iterations for series solutions when $\Lambda = 0.1$, $\beta_1 = 0.1$, $\beta_2 = 0.1$, $Fr = 0.3$, $Pr = 1$, $\gamma = 0.1$, $k_1 = 0.2$, $k_2 = 0.1$ and $Sc = 1$

Order of approximations	$-f''(0)$	$-g'(0)$	$-\theta'(0)$	$\phi'(0)$
1	1.0215	0.12667	0.088154	0.049515
5	1.0318	0.14819	0.085496	0.052571
10	1.0318	0.14886	0.085094	0.060685
15	1.0318	0.14877	0.085059	0.066513
20	1.0318	0.14888	0.085050	0.073378
25	1.0318	0.14888	0.085048	0.079135
30	1.0318	0.14888	0.085048	0.082693
35	1.0318	0.14888	0.085048	0.082693

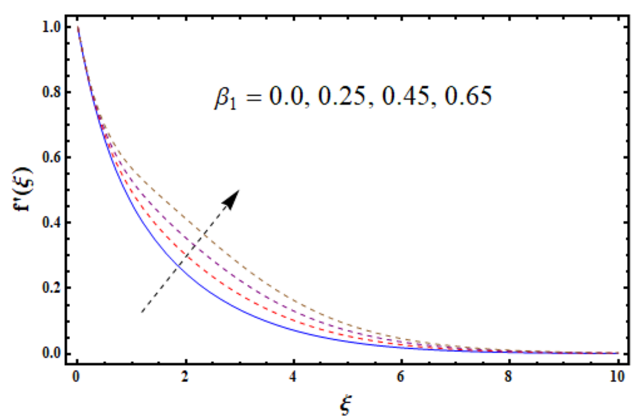

Fig. 4 f' versus β_1

variable on $g(\xi)$. Here we noticed that velocity component in y-direction upsurges versus larger Forchheimer number. It is also noticed that layer thickness enhances against larger Forchheimer number.

Behavior of Prandtl number on thermal field is recorded in Fig. 11. Lesser thermal field is noticed against higher Prandtl number. Characteristics of Biot number on thermal field is shown in Fig. 12. Here temperature is an increasing function of larger Biot number. Physically, larger Biot number increases the convection process at the stretchable surface which leads to upsurges the temperature field. Figure 13 predicts the salient attributes of heat generation/absorption or heat source/sink variable on the thermal field. In this study, $S > 0$ highlights the heat generation

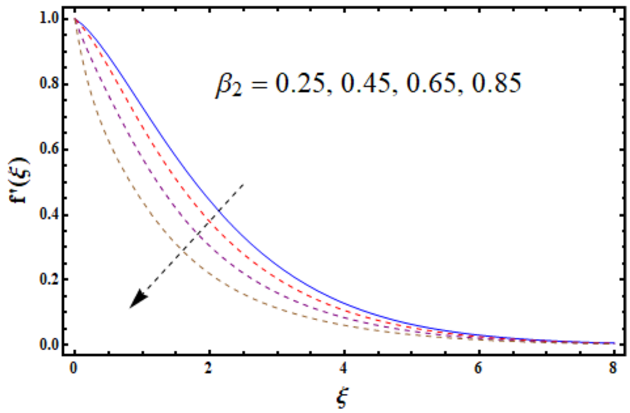

Fig. 5 f' versus β_2

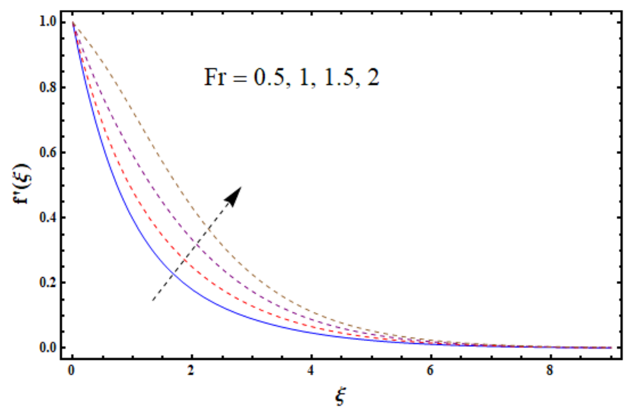

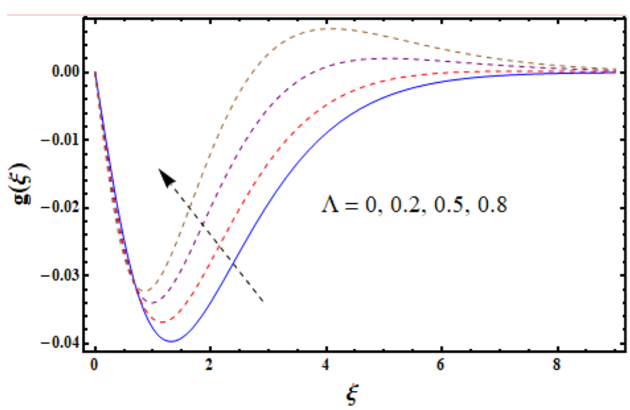

Fig. 6 f' versus Fr

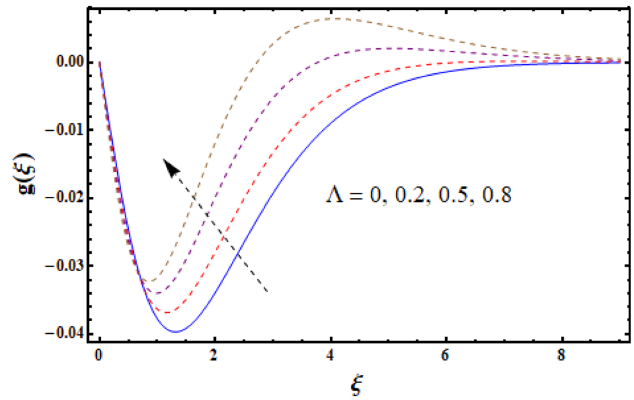

Fig. 7 g versus Λ

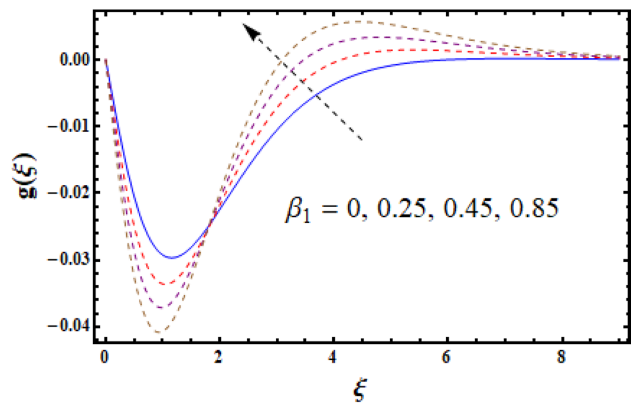

Fig. 8 g versus β_1

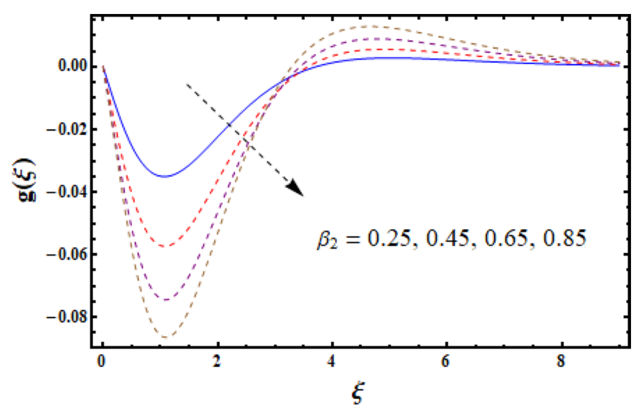

Fig. 9 g versus β_2

or heat source and $S < 0$ signifies the absorption or sink and $S = 0$ signposts there is no heat generation/absorption or heat source/sink. But here we have only presented the effect of heat generation on the thermal field. Thermal field is an increasing behavior against heat generation variable.

Figure 14 highlights the salient attributes of Schmidt number on mass concentration field. Physically, Schmidt number is the combination of momentum and mass diffusivity. Here mass concentration increases against higher Schmidt number. Also concentration layer thickness

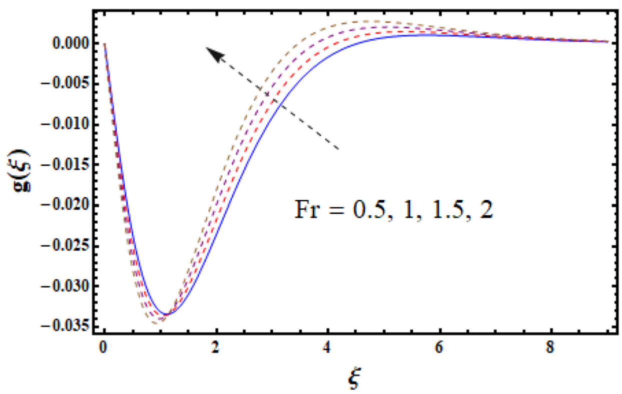

Fig. 10 g versus Fr

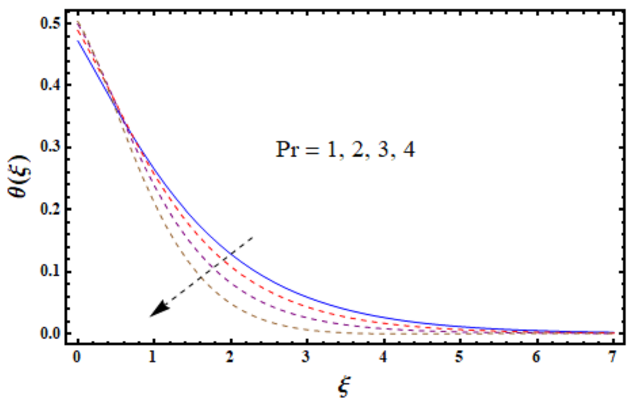

Fig. 11 θ versus Pr

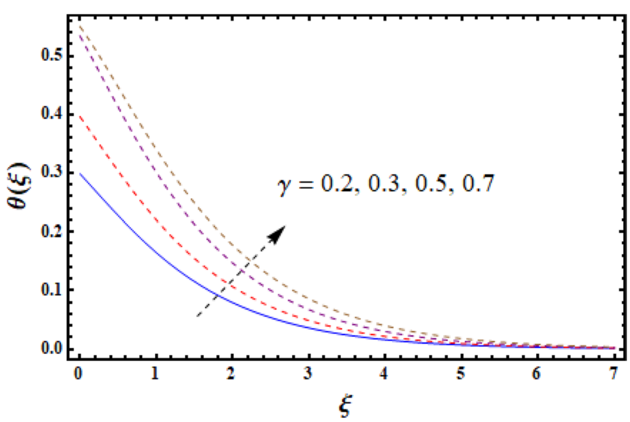

Fig. 12 θ versus γ

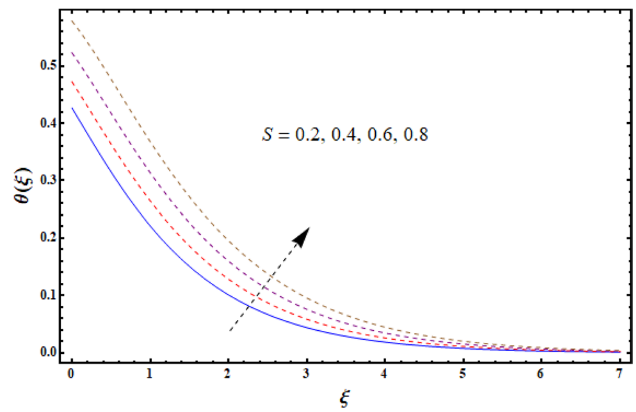

Fig. 13 θ versus S

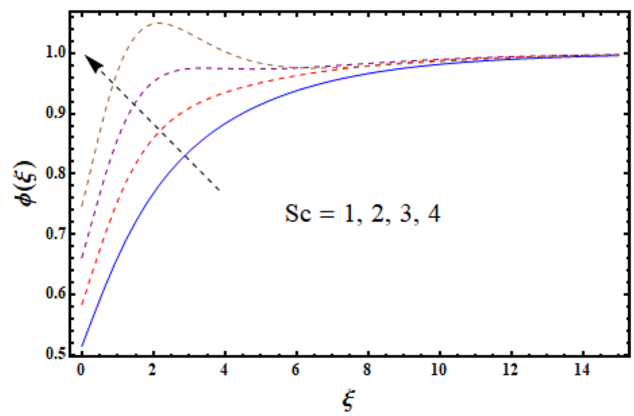

Fig. 14 ϕ versus Sc

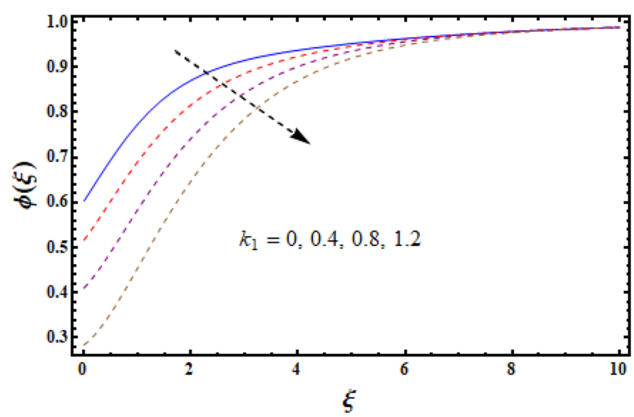

Fig. 15 ϕ versus k_1

upsurges versus rising estimations of Schmidt number. Attributes of homogeneous reactive variable on mass concentration is sketched in 15. Here we have examined reduction in solutal layer and as well as in mass concentration via higher homogeneous reactive variable. Behavior of heterogeneous reactive variable on mass concentration is revealed in Fig. 16. From this sketch, we have examined that concentration of reaction species at the surface upsurges against higher estimation of heterogeneous reactive variable.

Graphical sketch of heat transfer rate against various flow variables like porosity parameter, Biot number and

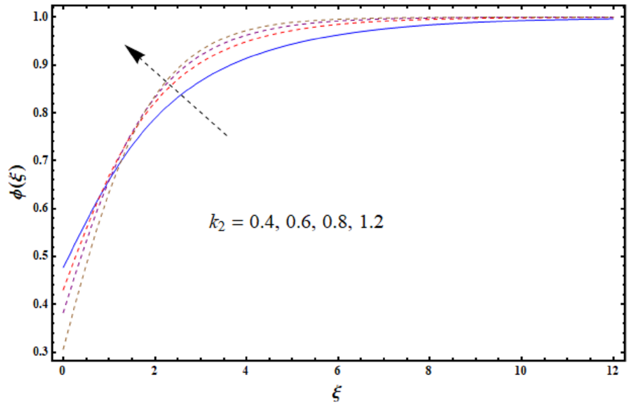

Fig. 16 ϕ versus k_2

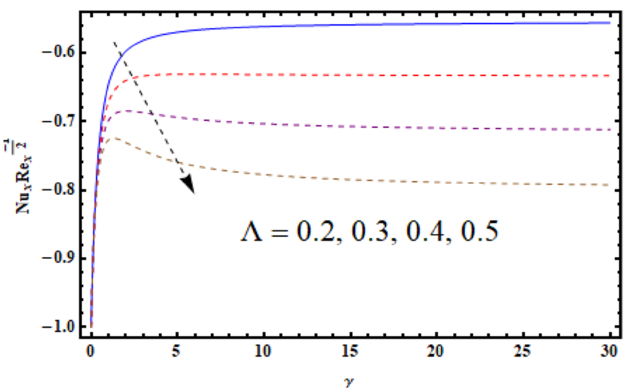

Fig. 17 Nusselt number versus Λandγ

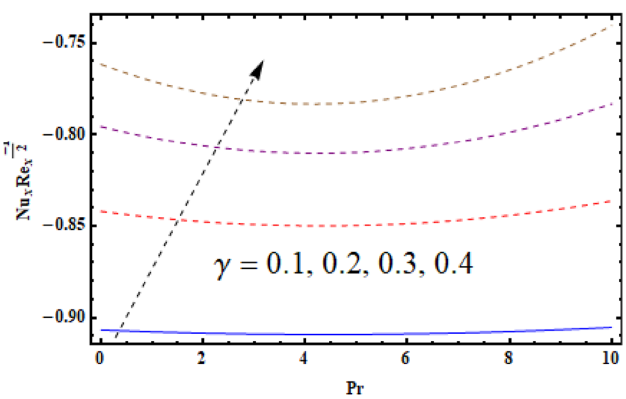

Fig. 18 Nusselt number versus γandPr

Prandtl number is highlighted in Figs. 17 and 18. From these sketches, we have noticed that magnitude of heat transfer decays versus higher estimations of porosity parameter and Biot number.

Concluding remarks

The valuable results of the presented problem are recorded below:

- Velocity of material particles in x direction decays against higher porosity variable.
- Velocity shows contrast impact against relaxation and retardation variables.
- Thermal declines versus Prandtl number.
- Higher heat generation variable upsurge the temperature of material particles.
- Concentration presents contrast impact against homogeneous and heterogeneous reactive parameters.
- Magnitude of heat transfer rate decays against larger porosity parameter and Biot number.

References

Abbasi FM, Shanakhat I, Shehzad SA (2019) Entropy generation analysis for peristalsis of nanofluid with temperature dependent viscosity and Hall effects. J Magn Magn Mater 474:434–441

Ahmad S, Khan MI, Hayat T, Khan MI, Alsaedi A (2018) Entropy generation optimization and unsteady squeezing flow of viscous fluid with five different shapes of nanoparticles. Colloids Surf A 554:197–210

Akbarzadeh M, Rashidi S, Karimi N, Ellahi R (2018) Convection of heat and thermodynamic irreversibilities in two-phase, turbulent nanofluid flows in solar heaters by corrugated absorber plates. Adv Powder Technol 29:2243–2254

Alamri SZ, Ellahi R, Shehzad N, Zeeshan A (2019) Convective radiative plane Poiseuille flow of nanofluid through porous medium with slip: an application of Stefan blowing. J Mol Liq 273:292–304

Das K, Chakraborty T, Kundu PK (2018) Effect of magnetic field on Oldroyd-B type nanofluid flow over a permeable stretching surface. Propuls Power Res 7:238–246

Ellahi R, Rahman SU, Nadeem S, Akbar NS (2014a) Blood flow of nanofluid through an artery with composite stenosis and permeable walls. Appl Nanosci 4:919–926

Ellahi R, Riaz R, Nadeem S (2014b) A theoretical study of Prandtl nanofluid in a rectangular duct through peristaltic transport. Appl Nanosci 4:753–760

Ellahi R, Hassan M, Zeeshan A, Khan AA (2016) The shape effects of nanoparticles suspended in HFE-7100 over wedge with entropy generation and mixed convection. Appl Nanosci 6:641–651

Fagbade AI, Falodun BO, Omowaye AJ (2018) MHD natural convection flow of viscoelastic fluid over an accelerating permeable surface with thermal radiation and heat source or sink: spectral homotopy analysis approach. Ain Shams Eng J 9:1029–1041

Gireesha BJ, Kumar KG, Ramesh GK, Prasannakumara BC (2018) Nonlinear convective heat and mass transfer of Oldroyd-B nanofluid over a stretching sheet in the presence of uniform heat source/sink. Results Phys 9:1555–1563

Han S, Zheng L, Li C, Zhang X (2014) Coupled flow and heat transfer in viscoelastic fluid with Cattaneo-Christov heat flux model. Appl Math Lett 38:87–93

Hashmi MS, Khan N, Mahmood T, Shehzad SA (2017) Effect of magnetic field on mixed convection flow of Oldroyd-B nanofluid induced by two infinite isothermal stretching disks. Int J Therm Sci 111:463–474

Hassan M, Marin M, Alsharif A, Ellahi R (2018) Convection heat transfer flow of nanofluid in a porous medium over wavy surface. Phys Lett A 382:2749–2753

Hayat T, Khan MI, Farooq M, Alsaedi A, Waqas M, Yasmeen T (2016a) Impact of Cattaneo-Christov heat flux model in flow of variable thermal conductivity fluid over a variable thicked surface. Int J Heat Mass Transf 99:702–710

Hayat T, Khan MI, Farooq M, Yasmeen T, Alsaedi A (2016b) Water-carbon nanofluid flow with variable heat flux by a thin needle. J Mol Liq 224:786–791

Hayat T, Khan MI, Waqas M, Alsaedi A (2017a) Effectiveness of magnetic nanoparticles in radiative flow of Eyring-Powell fluid. J Mol Liq 231:126–133

Hayat T, Waqas M, Khan MI, Alsaedi A, Shehzad SA (2017b) Magnetohydrodynamic flow of Burgers fluid with heat source and power law heat flux. Chin J Phys 55:318–330

Hayat T, Khan MI, Waqas M, Alsaedi A (2017c) Newtonian heating effect in nanofluid flow by a permeable cylinder. Results Phys 7:256–262

Hayat T, Khan MI, Waqas M, Alsaedi A (2017d) On Cattaneo-Christov heat flux in the flow of variable thermal conductivity Eyring-Powell fluid. Results Phys 7:446–450

Hayat T, Khan MWA, Alsaedi A, Khan MI (2017e) Corrigendum to "Squeezing flow of second grade liquid subject to non-Fourier heat flux and heat generation/absorption". Colloid Polym Sci 295:2439–2439

Hayat T, Qayyum S, Khan MI, Alsaedi A (2017f) Modern developments about statistical declaration and probable error for skin friction and Nusselt number with copper and silver nanoparticles. Chin J Phys 55:2501–2513

Hayat T, Khan MI, Qayyum S, Alsaedi A (2018a) Entropy generation in flow with silver and copper nanoparticles. Colloids Surf A 539:335–346

Hayat T, Khan MI, Qayyum S, Alsaedi A, Khan MI (2018b) New thermodynamics of entropy generation minimization with nonlinear thermal radiation and nanomaterials. Phys Lett A 382:749–760

Hayat T, Khan MI, Shehzad SA, Khan MI, Alsaedi A (2018c) Numerical simulation of Darcy-Forchheimer flow of third grade liquid with Cattaneo-Christov heat flux model. Math Methods Appl Sci 41:4352–4359

Hayat T, Ahmed S, Khan MI, Khan MI, Alsaedi A (2018d) A framework for heat generation/absorption and modified homogeneous-heterogeneous reactions in flow based through non-Darcy Forchheimer medium. Nucl Sci Technol 50:389–395

Hayat T, Khan MI, Khan TA, Khan MI, Ahmad S, Alsaedi A (2018e) Entropy generation in Darcy-Forchheimer bidirectional flow of water-based carbon nanotubes with convective boundary conditions. J Mol Liq 265:629–638

Khan N, Mahmood T (2016) Thermophoresis particle deposition and internal heat generation on MHD flow of an Oldroyd-B nanofluid between radiative stretching disks. J Mol Liq 216:571–582

Khan MI, Yasmeen T, Khan MI, Farooq M, Wakeel M (2016) Research progress in the development of natural gas as fuel for road vehicles: a bibliographic review (1991–2016). Renew Sustain Energy Rev 66:702–741

Khan MI, Waqas M, Hayat T, Alsaedi A (2017a) A comparative study of Casson fluid with homogeneous-heterogeneous reactions. J Colloid Interface Sci 498:85–90

Khan MI, Hayat T, Khan MI, Alsaedi A (2017b) A modified homogeneous–heterogeneous reactions for MHD stagnation flow with viscous dissipation and Joule heating. Int J Heat Mass Transfer 113:310–317

Khan MI, Waqas M, Hayat T, Khan MI, Alsaedi A (2017c) Behavior of stratification phenomenon in flow of Maxwell nanomaterial with motile gyrotactic microorganisms in the presence of magnetic field. Int J Mech Sci 132:426–434

Khan MI, Hayat T, Waqas M, Khan MI, Alsaedi A (2017d) Impact of heat generation/absorption and homogeneous-heterogeneous reactions on flow of Maxwell fluid. J Mol Liq 233:465–470

Khan MI, Khan MI, Waqas M, Hayat T, Alsaedi A (2017e) Chemically reactive flow of Maxwell liquid due to variable thicked surface. Int Commun Heat Mass Transfer 86:231–238

Khan MI, Waqas M, Hayat T, Alsaedi A, Khan MI (2017f) Significance of nonlinear radiation in mixed convection flow of magneto Walter-B nanoliquid. Int J Hydrogen Energy 42:26408–26416

Khan MI, Tamoor M, Hayat T, Alsaedi A (2017g) MHD Boundary layer thermal slip flow by nonlinearly stretching cylinder with suction/blowing and radiation. Results Phys 7:1207–1211

Khan MI, Alsaedi A, Shehzad SA, Hayat T (2017h) Hydromagnetic nonlinear thermally radiative nanoliquid flow with Newtonian heat and mass conditions. Results Phys 7:2255–2260

Khan NB, Ibrahim Z, Khan MI, Hayat T, Javed MF (2018a) VIV study of an elastically mounted cylinder having low mass-damping ratio using RANS model. Int J Heat Mass Transf 121:309–314

Khan MWA, Khan MI, Hayat T, Alsaedi A (2018b) Entropy generation minimization (EGM) of nanofluid flow by a thin moving needle with nonlinear thermal radiation. Phys B 534:113–119

Khan MI, Hayat T, Alsaedi A, Qayyum S, Tamoor M (2018c) Entropy optimization and quartic autocatalysis in MHD chemically reactive stagnation point flow of Sisko nanomaterial. Int J Heat Mass Transf 127:829–837

Khan MI, Hayat T, Khan MI, Waqas M, Alsaedi A (2019) Numerical simulation of hydromagnetic mixed convective radiative slip flow with variable fluid properties: a mathematical model for entropy generation. J Phys Chem Solids 125:153–164

Kumar KG, Ramesh GK, Gireesha BJ, Gorla RSR (2018) Characteristics of Joule heating and viscous dissipation on three-dimensional flow of Oldroyd B nanofluid with thermal radiation. Alex Eng J 57:2139–2149

Meraj MA, Shehzad SA, Hayat T, Abbasi FM, Alsaedi A (2017) Darcy-Forchheimer flow of variable conductivity Jeffrey liquid with Cattaneo-Christov heat flux theory. Appl Math Mech 2017(38):557–566

Muhammad T, Alsaedi A, Hayat T, Shehzad SA (2017) A revised model for Darcy-Forchheimer three-dimensional flow of nanofluid subject to convective boundary condition. Results Phys 7:2791–2797

Naghshband S, Araghi MAF (2018) Solving generalized quintic complex Ginzburg-Landau equation by homotopy analysis method. Ain Shams Eng J 9:607–613

Raftari B, Vajravelu K (2012) Homotopy analysis method for MHD viscoelastic fluid flow and heat transfer in a channel with a stretching wall. Commun Nonlinear Sci Numer Simul 17:4149–4162

Rashidi S, Akar S, Bovand M, Ellahi R (2018) Volume of fluid model to simulate the nanofluid flow and entropy generation in a single slope solar still. Renew Energy 115:400–410

Shehzad SA (2018) Magnetohydrodynamic Jeffrey nanoliquid flow with thermally radiative Newtonian heat and mass species. Rev Mex Fis 64:628–633

Shehzad SA, Alsaedi A, Hayat T, Alhuthali MS (2014) Thermophoresis particle deposition in mixed convection three-dimensional radiative flow of an Oldroyd-B fluid. J Taiwan Inst Chem Engineers 45:787–794

Shirkhani MR, Hoshyar HA, Rahimipetroudi I, Akhavan H, Ganji DD (2018) Unsteady time-dependent incompressible Newtonian fluid flow between two parallel plates by homotopy analysis method (HAM), homotopy perturbation method (HPM) and collocation method (CM). Propuls Power Res 7:247–256

Shivakumara IS, Dhananjaya M, Ng CO (2015) Thermal convective instability in an Oldroyd-B nanofluid saturated porous layer. Int J Heat Mass Transf 84:167–177

Skoneczny S, Skoneczny MC (2018) Mathematical modelling and approximate solutions for microbiological processes in biofilm through homotopy-based methods. Chem Eng Res Des 139:309–320

Tamoor M, Waqas M, Khan MI, Alsaedi A, Hayat T (2017) Magnetohydrodynamic flow of Casson fluid over a stretching cylinder. Results Phys 7:498–502

Turkyilmazoglu M (2010a) A note on the homotopy analysis method. Appl Math Lett 23:1226–1230

Turkyilmazoglu M (2010b) Purely analytic solutions of magnetohydrodynamic swirling boundary layer flow over a porous rotating disk. Comput Fluids 39:793–799

Turkyilmazoglu M (2014) Three dimensional MHD flow and heat transfer over a stretching/shrinking surface in a viscoelastic fluid with various physical effects. Int J Heat Mass Transf 78:150–155

Waqas M, Ijaz Khan M, Hayat T, Alsaedi A (2017a) Stratified flow of an Oldroyd-B nanoliquid with heat generation. Results Phys 7:2489–2496

Waqas M, Khan MI, Hayat T, Alsaedi A, Khan MI (2017b) Nonlinear thermal radiation in flow induced by a slendering surface accounting thermophoresis and Brownian diffusion. Eur Phys J Plus 132:280

Xinhui S, Liancun Z, Xinxin Z, Xinyi S (2012) Homotopy analysis method for the asymmetric laminar flow and heat transfer of viscous fluid between contracting rotating disks. Appl Math Model 36:1806–1820

Zhang Y, Zhang M, Bai Y (2016) Flow and heat transfer of an Oldroyd-B nanofluid thin film over an unsteady stretching sheet. J Mol Liq 220:665–670

Zhang Y, Yuan B, Bai Y, Cao Y, Shen Y (2018) Unsteady Cattaneo-Christov double diffusion of Oldroyd-B fluid thin film with relaxation-retardation viscous dissipation and relaxation chemical reaction. Powder Technol 338:975–982